Granular segregation induced by a moving subsurface blade

Vidushi Dwivedi,[1] Julio M. Ottino,[1,2,3] Richard M. Lueptow,[1,2,3] and Paul B. Umbanhowar[3,*]
[1]*Department of Chemical and Biological Engineering, Northwestern University, Evanston, Illinois 60208, USA*
[2]*The Northwestern Institute on Complex Systems (NICO), Northwestern University, Evanston, Illinois 60208, USA*
[3]*Department of Mechanical Engineering, Northwestern University, Evanston, Illinois 60208, USA*

(Received 25 May 2019; published 8 November 2019)

Size-driven particle segregation can occur when an object such as a blade moves through an otherwise static bed of granular material. Here we use discrete element method (DEM) simulations to study segregation resulting from a subsurface blade moving through a bed of size-bidisperse spherical particles. Segregation increases with each pass of the blade until a surface layer of mostly large particles forms above a small-particle layer adjacent to the bottom wall. The rate of segregation decreases with each pass so that the degree of segregation asymptotically approaches its maximum value, and the number of passes to reach a steady segregation state increases as the bed depth is increased or the blade height decreased. In shallow beds, the characteristic number of passes for segregation, τ, scales with the inverse of the granular inertial number, I. In deep beds with small blade heights, the effect of the blade is more localized to its immediate vicinity, resulting in many more passes of the blade to reach a steady segregation state, and a corresponding deviation from the shallow bed scaling of τ with I^{-1}.

DOI: 10.1103/PhysRevE.100.052902

I. INTRODUCTION

Granular materials differing in size, density, shape, or other physical properties frequently segregate, or "de-mix," upon excitation. For example, size segregation occurs when small particles fall between large particles resulting in regions of mostly small particles below regions of mostly large particles. This can occur due to excitation in the form of vibration or flow. Vibration-induced segregation, sometimes referred to as the "Brazil nut effect," is the result of complicated interactions between the vibrational excitation, friction at walls, convection rolls, and the interstitial fluid [1,2]. Flow-induced segregation, which is considered here, depends on the interplay between advection, collisional diffusion, and the tendency for the particles to segregate [3–5]. While many studies have considered segregation in gravity-driven surface flows such as chutes, heaps, rotating tumblers, and landslides [3–5], few have considered granular segregation resulting from flow due to the motion of an intruder such as a moving blade, which we consider here.

In flowing granular systems, whether driven by gravity or the motion of an intruder, size segregation is the result of "kinetic sieving" in which small particles preferentially fall into shear-generated voids and both small and large particles are pushed upward by particles below them through "squeeze explusion" [6]. Recent work suggests the additional importance of a shear mechanism [7].

The segregation mechanism is often characterized by a segregation, or percolation, velocity relative to the local bulk velocity that depends on the local species concentration and some measure of the disruption of otherwise static particles such as the shear rate [6,8,9], the slope of the free surface of the particle bed driving the flow [10], or the local stress field [11]. Most research on segregation in flowing granular mixtures has focused on relatively shallow gravity-driven free surface flows such as those that occur in heaps, chutes, and tumblers [3,4,6,12–14]. However, scenarios exist where segregation can occur when otherwise static particles are disturbed by the motion of objects such as mixer blades [15–17], tines [18], and plows [19,20], or by the movement of a burrowing or surface locomoting organism or device [21]. Here we consider segregation induced from a moving subsurface blade.

Much of the previous research examining an object moving through a bed of particles focuses on the forces on the object or the localized motion of particles near the object. Monodisperse granular flows over blades have been examined to study forces on the blade as function of packing fraction [22] and blade angle [23], as well as mixing of the particles [24]. Flow of granular materials around objects is relevant to a number of industrial processes that involve cylindrical mixers with rotating bladed impellers used to homogenize solid particle blends. Previous experimental and computational research considered kinematics and mixing in bladed mixers by employing monodisperse systems [19,20,25]. A handful of studies have explored the effect of particle size differences on flow and segregation in bladed mixers [17,26,27]. In these cases, as well as most monodisperse cases mentioned above, the blade height is nearly equal to the bed depth, and the velocity field is examined in the surface bump that results from the movement of the blade through the bed of particles. Typically, a three-dimensional recirculating flow develops around each blade [17]. However, details of the segregation and its dependence on bed depth and blade height have not been examined systematically, despite their practical importance. The objective here is to understand the segregation resulting from a submerged blade moving through a bed of size bidisperse particles.

*Corresponding author: umbanhowar@northwestern.edu

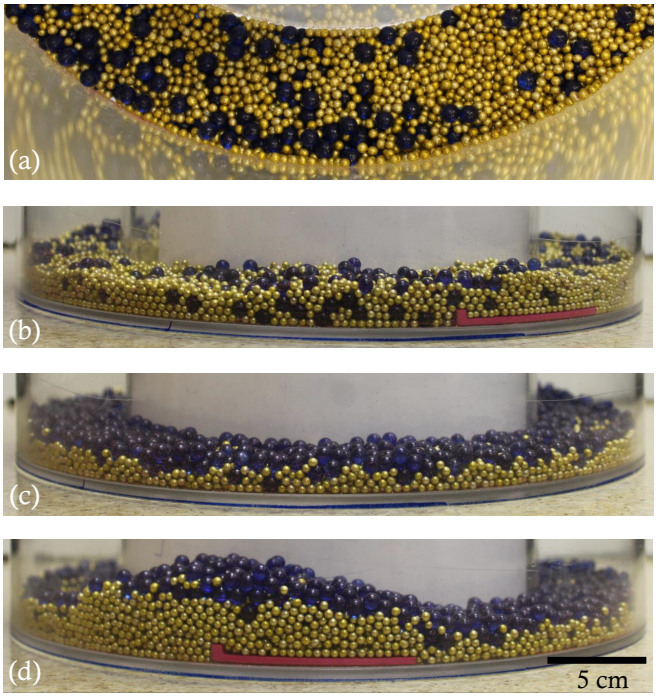

FIG. 1. Annulus with an equal volume mixture of 5.98 ± 0.06 mm diameter (blue) and 3.12 ± 0.13 mm diameter (gold) glass particles and a subsurface blade (red). (a) Top view and (b) side view of initial condition. Segregation after ten passes (c) opposite the blade and (d) in the bump above the blade for clockwise blade motion when viewed from above (right to left in the image).

To qualitatively demonstrate how a moving subsurface blade causes a bed of initially mixed size-bidisperse particles to segregate, an annulus with an inner diameter of 19.5 cm and an outer diameter of 29.1 cm is filled with an equal volume mixture of large (blue) and small (gold) glass beads having diameters $d_L = 5.98 \pm 0.06$ mm and $d_S = 3.12 \pm 0.13$ mm, respectively, such that the initial height of the particle bed h is about five times the blade height h_b. An $h_b = 0.72$ cm blade is moved manually through the bed of mixed particles N times using a magnet attached to the bottom surface of the blade coupled to another magnet below the flat bottom surface of the annulus. Figure 1(a) shows a top view of a section of the annulus with the initial condition of mixed particles, while Fig. 1(b) shows a corresponding side view with the side of the blade (red) visible. The initial condition is not perfectly mixed as a small particle rich layer forms at the bottom wall during bed preparation. This only marginally affects segregation measurements, as mentioned later. After ten passes of the blade ($N = 10$), the mixture is well segregated, as evident by the large-particle surface layer and small-particle base layer visible in Fig. 1(c). In addition, as shown in Fig. 1(d), a large bump forms in the vicinity of the blade as it moves through the shallow particle bed.

In this paper, we use discrete element method (DEM) simulations to quantify the segregation resulting from a subsurface vertical wall "blade" moving through a bed of size-bidisperse spherical particles. This research differs from previous studies of segregation in two- or four-bladed mixers [15,17,26,27] in several ways. First, both the blade height and bed depth are varied, with the blade height always less than the nominal bed depth. Most previous studies with mixers fix the blade height and then fill the mixer such that the particles just cover the blades [15,17,19,26,27]. Second, we use an effectively two-dimensional geometry rather than the cylindrical geometry used in previous bladed mixer work [15,17,19,26,27]. This allows us to study the segregation phenomenon in a simpler configuration. Moreover, the primary concern in this study is the nature of the segregation from a fundamental standpoint, rather than replicating conditions in industrial mixers.

Details of the geometry and DEM simulations are described in Sec. II and the Appendix. In Sec. III, simulation results show the impact of varying the bed depth and blade height on segregation as well as details of the local flow and segregation around the blade. In Sec. IV, the work is summarized and extensions are proposed.

II. SIMULATION METHODS

DEM simulations, details of which are provided in the Appendix, are performed in a particle bed of depth h with periodic boundaries in the streamwise (z) and spanwise (x) directions. The blade is a horizontally moving vertical wall of height h_b that spans the width of the bed and contacts the bottom wall. It translates from left to right in the streamwise (z) direction at a constant blade velocity of $v_b = 0.1$ m/s. The acceleration due to gravity in the vertical y direction is $g = -9.8\ \mathrm{m/s^2}$.

The initially well-mixed bed consists of an equal volume mixture of large ($d_L = 8$ mm) and small ($d_S = 4$ mm) spherical particles with a size ratio of $d_L/d_S = 2$. Each particle species has a uniformly distributed size polydispersity of $\pm 10\%$ to reduce particle ordering. For a specified bed length L_z, the bed depth h is controlled by changing the number of particles. Since the effect of the blade is localized to regions immediately in front of and behind the blade, L_z is kept long enough that disturbances in front of the moving blade do not overlap those behind the blade due to the streamwise periodic boundary conditions. This requires $L_z \approx 9.5h$ for $h = 5.7d_L$ and $h = 11d_L$. In deeper beds, the disturbed zone is more localized, so $L_z \approx 6.5h$ for $h = 16.3d_L$.

The periodic bed width (spanwise) is $L_x = 6d_L$ for all cases. Simulation of systems having double this width, i.e., $L_x = 12d_L$, yield quantitatively similar results. The bottom wall and blade consist of a single layer of spherical particles with diameter $d_{\mathrm{wall}} = 2.2$ mm $< d_s$ to provide a rough surface while avoiding large depressions between wall particles that might overly restrict the motion of the bed particles. To consider the simplest case, the blade extends vertically (rather than at an angle) from the bottom wall. The blade spans the bed width (L_x), and its height h_b is measured from the top of the bottom wall particles to the top of the blade. Note that h_b may be a noninteger multiple of the wall particle diameter because the lower part of the blade is allowed to computationally pass through particles forming the wall. The blade height is varied, but is smaller than the bed depth for all cases. The number of particles in the simulations varies from 15 000 to 72 000, depending on h and L_z.

Initially, the blade is at rest at the extreme left of the domain ($z = 0$), as shown in Fig. 2. Large and small particles are

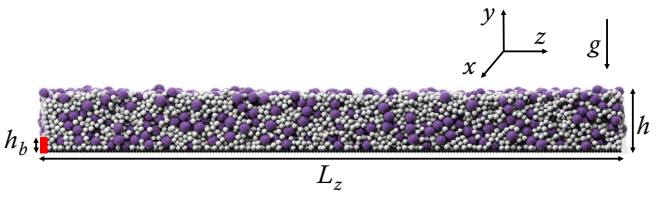

FIG. 2. Side-view of DEM simulation showing a blade of height h_b (at the left end) in an initially mixed bed of particles of depth h consisting of equal volumes of large ($d_L = 8$ mm) and small ($d_S = 4$ mm) particles. Periodic boundary conditions are maintained in the streamwise (z) and spanwise (x) directions. Gravity acts in the downward vertical direction (y). The blade translates in the positive streamwise direction, i.e., from left to right, at $v_b = 0.1$ m/s.

randomly assigned to nodes in a uniform three-dimensional grid above the bottom wall. At $t = 0$, gravity is turned on, and particles fall to generate a random mixture of particles supported by the bottom wall. The particles settle within $t \approx 2$ s. At $t = 3$ s, the blade is translated horizontally in the positive streamwise direction at $v_b = 0.1$ m/s, a velocity low enough to avoid inertial effects and maintain persistent contacts between particles, while large enough to minimize simulation time. When the blade travels the entire length of the domain and exits the system on the right ($z = L_z$), one "pass" is complete. The blade reenters the domain for the next pass from the left end ($z = 0$). Since the blade spans the entire bed width, the average particle flux in the spanwise direction is zero, and the system is effectively two-dimensional.

III. RESULTS

A. Shallow beds

1. Quantifying segregation

We consider first shallow bed systems where the effect of the submerged blade reaches the surface of the bed. Figure 3 shows a typical sequence of developing segregation with an increasing number of passes N for $h = 5.7d_L$ and $h_b = 1.14d_L$ ($h/h_b = 5$). When the blade begins to move, particles flow

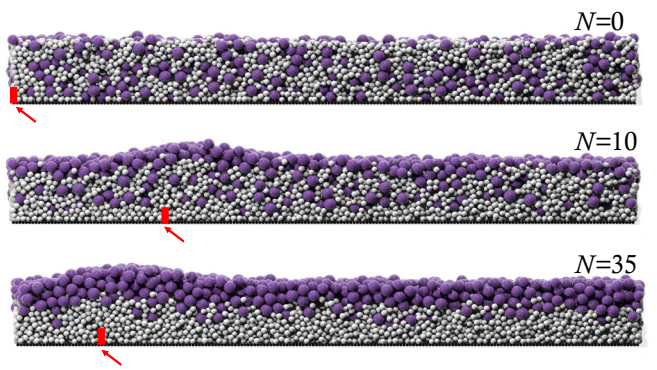

FIG. 3. Segregation evolution with number of passes N for $h = 5.7d_L$ and $h_b = 1.14d_L$ ($h/h_b = 5$) at (top) $N = 0$ before the blade starts to move, (middle) $N = 10$ as large particles accumulate at the top surface and small particles accumulate near the bottom wall, and (bottom) $N = 35$ when the system has segregated into two distinct layers. Red arrows indicate the blade position in each frame.

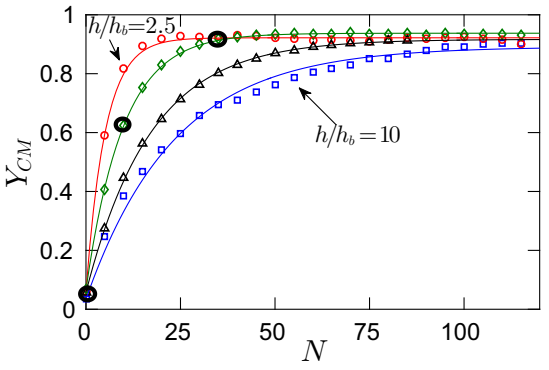

FIG. 4. Segregation metric Y_{CM} vs N for fixed $h = 5.7d_L$ and $h/h_b = 2.5, 5, 8, 10$. Segregation is slower for shorter blades (large h/h_b), but all the systems eventually reach a similar steady state value of $Y_{\mathrm{CM}} \approx 0.9$. Curves are best fits to Eq. (2).

over the blade. However, the system is long enough that particles far from the blade remain static. A bump forms on the free surface above the blade with its center slightly ahead of the blade, evident at $N = 10$ and $N = 35$ in Fig. 3 and consistent with previous results in a bladed mixer [15,25]. By $N = 10$, significant segregation has already occurred, with a decrease in concentration of large particles at the bottom of the bed and an increase in concentration of large particles at the free surface. By $N = 35$, the system has segregated into two layers with a slightly diffuse interface between them and a few stray particles of the opposite size in each layer.

To characterize the evolution of segregation with the number of passes of the blade, we calculate a segregation metric Y_{CM} using the relative center-of-mass height of the large particle species in the region excluding the streamwise span of the bump over the blade. For each pass, Y_{CM} is calculated as

$$Y_{\mathrm{CM}} = \frac{y_L/y_{\mathrm{CM}} - 1}{1 - c_L}, \tag{1}$$

where y_L (y_S) is the mean height of large (small) particles with respect to the top of the rough bottom wall, c_L (c_S) is the volume concentration of large (small) particles in the region excluding the bump, and the center of mass of the entire bed is $y_{\mathrm{CM}} = y_L c_L + y_S(1 - c_L)$, assuming $c_L + c_S = 1$. All heights are measured with respect to the tops of the bottom wall particles. For a well mixed particle bed, $Y_{\mathrm{CM}} = 0$; for a completely segregated bed, $Y_{\mathrm{CM}} = 1$.

Y_{CM} is plotted as a function of N in Fig. 4 for the system depicted in Fig. 3 as well as several other cases. Y_{CM} for the passes shown in Fig. 3 are marked with black circles around the data points. The initial ordering of small particles near the bottom wall in the experimental setup shown in Fig. 1 also occurs in the simulations. This results in a small deviation in Y_{CM} from the perfectly mixed initial condition of $Y_{\mathrm{CM}} = 0$ at $N = 0$. With increasing N, Y_{CM} increases as the center of mass of large particles rises, consistent with the ongoing segregation. The segregation rate is higher for the initial passes and decreases in subsequent passes as the system approaches the final steady state segregation. After $N \approx 40$, the segregation reaches a steady state.

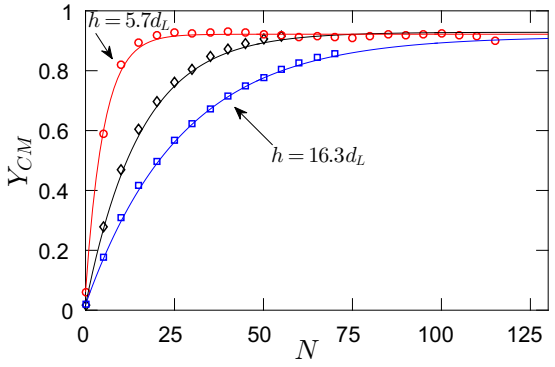

FIG. 5. Dependence of Y_{CM} on N for fixed $h/h_b = 2.5$ with $h/d_L = 5.7$, 11, 16.3. Deeper beds (larger h) take longer to segregate, although steady state values of Y_{CM} are nearly equal. Curves are best fits to Eq. (2).

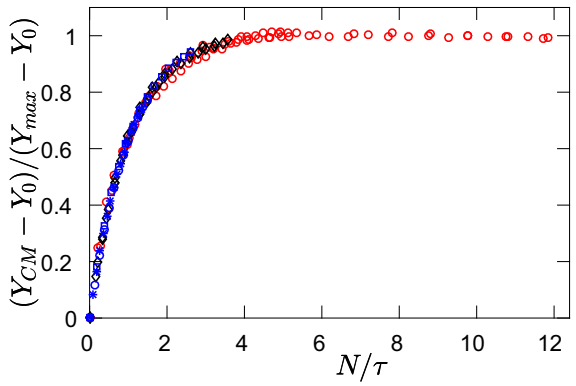

FIG. 6. Ten data sets for varying h/h_b and h collapse onto a single curve when Y_{CM} is scaled to lie between 0 and 1 and the number of passes N is scaled by the characteristic number of passes τ. Red symbols: $h = 5.7d_L$ ($h/h_b = 2.5, 5, 8, 10$); black symbols: $h = 11d_L$ ($h/h_b = 2.5, 4, 5$); and blue symbols: $h = 16.3d_L$ ($h/h_b = 2.5, 4, 5$).

To better understand the dependence of segregation on blade height h_b, the initial bed depth is fixed at $h = 5.7d_L$ and the blade height is varied from $0.57d_L$ to $2.28d_L$ ($2.5 < h/h_b < 10$), as shown in Fig. 4. The simulation with the shortest blade (largest h/h_b) requires the most passes ($N \approx 120$) to achieve steady state segregation, whereas the simulation with the tallest blade (smallest h/h_b) segregates the fastest ($N \approx 20$). The steady state value of Y_{CM} varies slightly between cases (0.89–0.94) because of the somewhat diffuse interface between the large and small particle layers in the fully segregated steady state. It decreases slightly as the blade height decreases, likely as a result of reduced influence of the smaller blade on particles well above it. The fast initial segregation in all cases comes about in two ways. First, as particles in regions in front of the blade are pushed up and over the blade, particles near the blade segregate, as will be discussed later. Second, segregation also occurs at the surface bump as the static bed is disrupted, forcing particles to flow down the trailing surface of the bump. Of course, segregation of one species depends on the local concentration of the other species, as has been shown in previous studies [8], which results in a decrease in the segregation rate with increasing segregation.

It is also interesting to vary the initial bed depth h and blade height h_b proportionally (i.e., fixed h/h_b), because a deeper bed results in increasing overburden pressure, which has been shown to decrease the segregation rate as well as the ultimate degree of segregation [28,29]. Figure 5 shows the dependence of Y_{CM} on N at $h/h_b = 2.5$ for h ranging from $5.7d_L$ to $16.3d_L$. All the systems reach a similar steady state segregation value ($Y_{\mathrm{CM}} \approx 0.9$), but the number of passes to reach the segregated state increases with increasing depth h.

At this point it is helpful to consider the general nature of the segregation development. In all the cases, Y_{CM} initially rises rapidly and then asymptotically approaches a final value near one. Since it appears that the final value for Y_{CM} is approached exponentially, we fit the evolution of Y_{CM} with N to

$$Y_{\mathrm{CM}} = (Y_{\mathrm{max}} - Y_0)(1 - e^{-N/\tau}) + Y_0, \qquad (2)$$

where τ is a characteristic number of passes, Y_0 is the measured initial value for Y_{CM} at $N = 0$, and Y_{max} is the maximum value for Y_{CM} at large N. Y_{max} and τ are the two fitting parameters. Curves fit to this equation are shown in Figs. 4 and 5, indicating that the evolution of Y_{CM} is well characterized by the exponential model.

Using Eq. (2), data sets for ten different bed depths and blade heights, including those shown in Figs. 4 and 5, can be collapsed onto a single curve when $(Y_{\mathrm{CM}} - Y_0)/(Y_{\mathrm{max}} - Y_0)$ is plotted versus N/τ, as shown in Fig. 6. This collapse indicates that all the cases share the same underlying segregation mechanism in the presence of the blade.

The dependence of τ on h and h_b for data sets shown in Figs. 6 is plotted in Fig. 7 for three different bed heights and a range of blade heights. The figure shows that segregation slows (τ increases) with increasing h/h_b (shorter blade) at fixed bed height, and that segregation in deeper beds is always slower (τ is greater) than in shallow beds at the same h/h_b value. The fastest segregation occurs when h and h/h_b are smallest. For the cases studied here, this occurs when $h = 6d_L$, and $h/h_b = 2.5$, for which nearly complete segregation occurs within 15 passes, corresponding to $\tau = 5.1$. In contrast, when $h = 16.3d_L$, and $h/h_b = 2.5$, $\tau = 26.3$ indicating that segregation is more than five times slower.

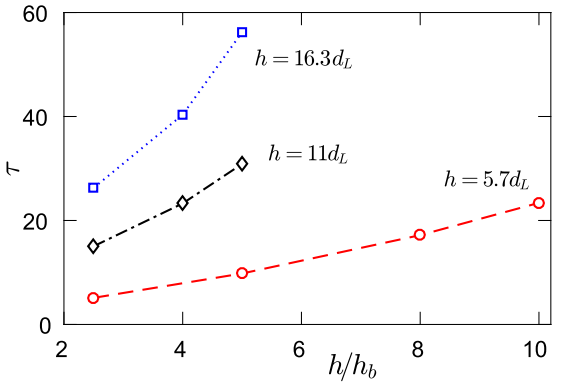

FIG. 7. Variation of characteristic number of passes τ with bed depth and blade height for ten simulations. Larger τ signifies slower segregation.

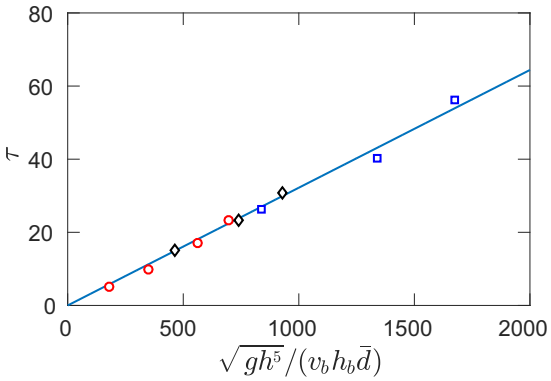

FIG. 8. In shallow beds, the characteristic number of passes τ increases linearly with $\sqrt{gh^5}/(v_b h_b \bar{d})$, which is closely related to the inverse of the dimensionless granular inertial number, $I = \dot{\gamma}\bar{d}/\sqrt{P/\rho}$.

It has been shown previously that the characteristic displacement timescale for a particle relative to the shear timescale of the flow can be represented by the granular inertial number, $I = \dot{\gamma}\bar{d}/\sqrt{P/\rho}$, where $\dot{\gamma}$ is the shear rate, $\bar{d}$ is the mean particle diameter, P is the local pressure, and ρ is the particle density [30]. Since segregation increases with increasing shear rate [6,8], we would expect τ to be inversely proportional to I. For the flow considered here, P can be estimated as the lithostatic pressure at the bottom of the bed ρgh and $\dot{\gamma}$ as v_{char}/h, where the characteristic velocity in the disturbed region around the blade, v_{char}, is assumed proportional to $v_b h_b/h$ (as confirmed in the next subsection). Thus, we would expect

$$\tau \propto 1/I = \sqrt{P/\rho}/\dot{\gamma}\bar{d} \propto \frac{\sqrt{gh^5}}{v_b h_b \bar{d}}. \tag{3}$$

Plotting the data in Fig. 7 according to this relation for τ (using $\bar{d} = 6$ mm) confirms that the dependence of τ on bed depth and blade height is accurately described by a linear function of the inverse of the inertia number, as shown in Fig. 8.

The relation in Fig. 8 is not unexpected in that a smaller inertial number [larger $\sqrt{gh^5}/(v_b h_b \bar{d})$] corresponds to a tendency toward quasistatic flow that should slow the segregation, resulting in a greater characteristic number of passes τ. In contrast to the strong dependence of τ on h and h_b (as well as I), we note that $Y_{\text{max}} \approx 0.9$ for all values of h and h_b examined. That is, regardless of the details of the blade and flow conditions, the particle bed is nearly fully segregated, with the deviation from perfect segregation ($Y_{\text{max}} = 1$) due to the inherent diffuse interface between the layers. However, as in other segregating flows, Y_{max} is expected to be a function of the particle size ratio, e.g., $Y_{\text{max}} = 0$ for $d_L/d_S = 1$ and $Y_{\text{max}} \to 1$ for large d_L/d_S.

2. *Segregation kinematics*

To identify the portion of the flow that drives the segregation, we consider both the local velocity field around the blade and individual particle trajectories. To calculate the velocity field, the bed is divided into cells of length d_S in the depth and streamwise directions and $6d_L$ (full width) in the spanwise direction. The average velocity in each cell is calculated over 0.1 s intervals for the duration of one pass. Then all instances of the velocity field are aligned to the blade and averaged, thereby providing an ensemble averaged velocity field in the region surrounding the blade over one pass.

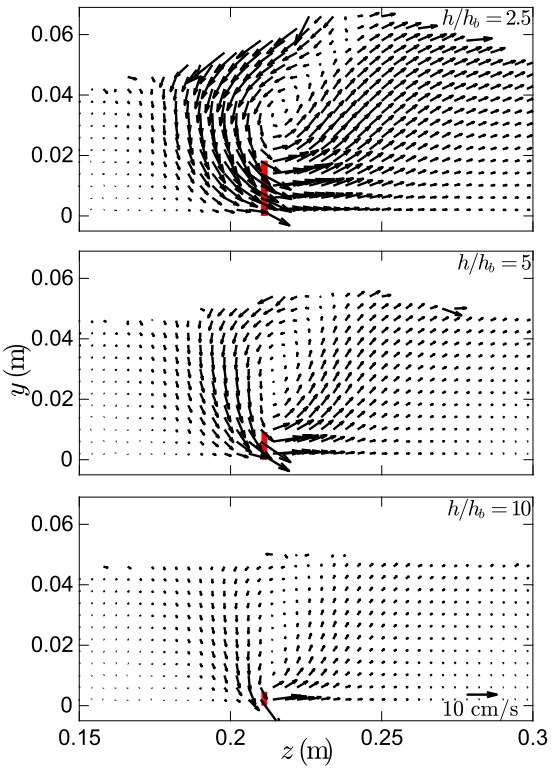

FIG. 9. Velocity field at $N = 5$ as the blade moves from left to right for various blade heights with fixed bed height $h = 5.7d_L$. Blade height and location are indicated by the red vertical line. Vector scale is shown at lower right of the bottom figure.

Figure 9 shows the velocity fields for simulations with three different blade heights ($h/h_b = 2.5$, 5, 10) and fixed $h = 5.7d_L$ at $N = 5$ evaluated in the stationary laboratory frame of reference but centered on the blade. The blade creates a finite zone of velocity disturbances around it, beyond which particles are static; this is consistent with previous bladed mixer studies [24,25]. For all three blade heights, particles above and in front of the blade are pushed forward and upward, while particles above and behind the blade fall downward and forward to fill in from behind. The latter results in a negative streamwise velocity at the free surface on the back (left) side of the bump. Particles immediately in front of and just behind the blade have the largest velocity with a magnitude nearly equal to the streamwise velocity of the blade, 0.1 m/s, which is again consistent with findings for bladed mixers [17]. Since particles behind the blade have a downward velocity as they fill the space created by the moving blade, and particles in front of the blade are pushed upward, the resulting movement is much like the recirculation that occurs in bladed mixers [17,19,20,25].

Comparing the velocity fields for different blade heights in Fig. 9, it is clear that a taller blade establishes a larger

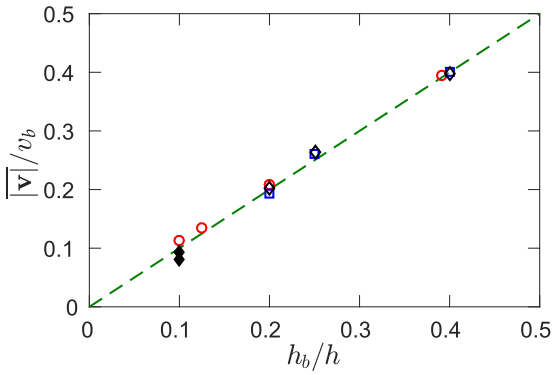

FIG. 10. Mean particle speed normalized by blade speed $\overline{|\mathbf{v}|}/v_b$ varies linearly with normalized blade height h_b/h for all shallow bed simulations (open symbols, same as earlier plots) as well as deep bed simulations (filled symbols, see Sec. III B).

high-velocity region. The higher velocities result in higher local shear rates, which allow more particle rearrangements per pass that have a direct correlation with the percolation velocity associated with segregation [8,9]. The surface bump is also higher for taller blades, as is evident from comparing the upper surfaces of the velocity vector plots in Fig. 9. As a result, particles with negative streamwise and vertical velocities on the back (left) side of the bump flow down a slope. As they do so, segregation occurs due to kinetic sieving as voids are created into which small particles are more likely to fall [10]. As a result of these two effects, segregation is greater for larger blade heights (smaller h/h_b), as shown in the previous section.

To quantify these observations regarding the velocity field, Fig. 10 plots the mean particle speed normalized by the blade velocity, $\overline{|\mathbf{v}|}/v_b$, as a function of the relative blade height, h_b/h, over one pass at $N = 5$. The averaging region extends through the depth of the layer and a lateral distance of $3.1h$ centered on the blade (slightly more than the entire frame shown in Fig. 9). Noting that $\overline{|\mathbf{v}|}$ characterizes the velocity in the disturbed region around the blade, Fig. 10 supports the assumption that $v_{\text{char}} \propto v_b h_b/h$ and, thereby, that τ scales as the inverse of the inertia number [Eq. (3)].

It is also instructive to consider individual particle trajectories during a single pass for particles starting at different initial heights y_0. To accomplish this, small and large particles within specific height ranges and within a fixed range of streamwise positions with respect to the blade are tracked during the fifth pass of the blade ($N = 5$). In Fig. 11, the vertical axis shows the vertical displacement from the initial height, $y - y_0$, normalized by the blade height h_b. The horizontal axis indicates the streamwise displacement from z_0, which corresponds to the streamwise location where the particle is highest in the bed, normalized by h_b. The first column shows the trajectories at the (a) top ($0.877 \leqslant y_0/h \leqslant 0.885$), (b) middle ($0.614 \leqslant y_0/h \leqslant 0.622$), and (c) bottom ($0.177 \leqslant y_0/h \leqslant 0.185$) portions of the bed for $h = 5.7d_L$ and the tallest blade, $h/h_b = 2.5$. Similarly, the second and third columns show the trajectories for simulations with $h/h_b = 5$ and $h/h_b = 10$, respectively, at the same heights noted above. Dashed red curves represent the trajectories of small particles, while solid blue curves represent the trajectories of large particles.

Figure 11 shows that particles are displaced both vertically and horizontally as the blade passes. The vertical displacement of the particles is approximately $1.5h_b$, independent of blade height or vertical position in the bed. Thus, the vertical displacement of particles scales with h_b through the entire depth of the bed. The horizontal displacement increases deeper in the bed. That is, the particles closest to the bottom of the bed are displaced a longer streamwise distance than those higher in bed, most likely because the particles deep in the bed are immediately adjacent to the blade. However, the blade-height normalized streamwise displacement is larger for a

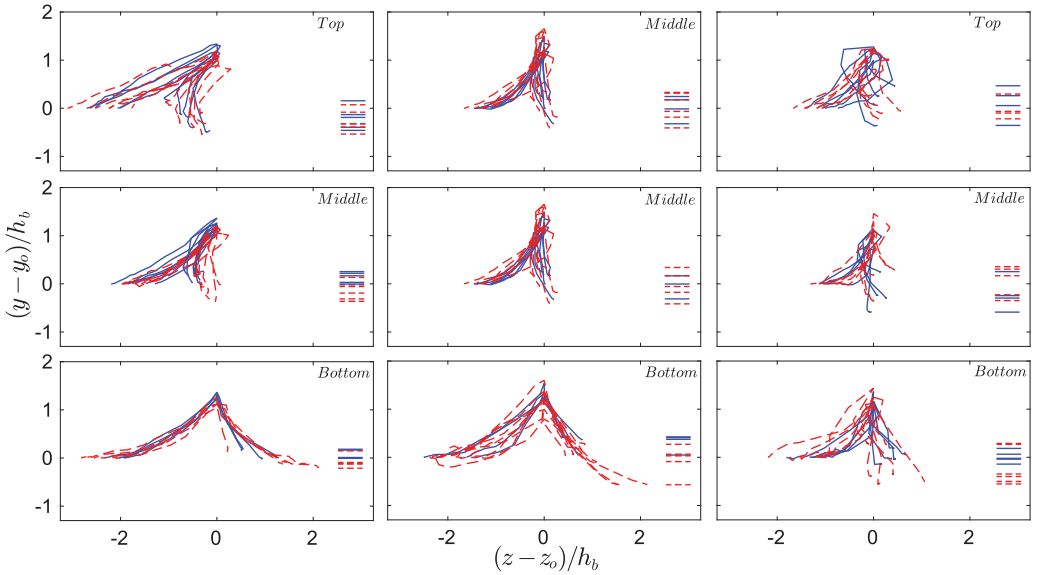

FIG. 11. Particle trajectories at different bed heights (rows, see text) during the $N = 5$ pass for fixed $h = 5.7d_L$ and varying h_b (columns, $h/h_b = 2.5$, 5, and 10 from left to right). Large (small) particle trajectories are shown in solid blue (dashed red). Horizontal lines indicate final heights of particles after blade passes.

taller blade ($h/h_b = 2.5$), meaning that a taller blade impacts a larger region of the bed in front of and behind the blade than a shorter blade, even when scaled by the blade height in Fig. 11.

In all cases, trajectories near the bottom of the bed are simple, consisting of a steady rise then fall as the particle is pushed forward. In contrast, particles higher in the bed often follow a looping trajectory (e.g., Fig. 11 for $h/h_b = 2.5$ and 5) where they move to the right and upward but then move slightly to the left and downward as the blade passes below them. All trajectories show clear signs of segregation, as indicated by the horizontal lines that mark the vertical position of each particle after the blade has passed. That is, generally, large particles (blue) end up above small particles (red) after the blade passes, even though both particle types start at the same vertical position before the blade passes.

At first glance, the net horizontal displacement of all particles with each pass seems to contradict the notion that there is no particle motion far from the blade. However, a simple control volume analysis resolves this apparent contradiction. Consider a fixed control volume that is long enough to include the length of the bump above the blade and is located midway between the streamwise periodic boundaries. As the bump enters the control volume, the volume of particles increases in the control volume, reaching a maximum when the bump is completely within the control volume. Hence, particles pass into the control volume from the left even though particles on the right side of the control volume are static. Likewise, as the bump passes out of the control volume, the volume of particles in the control volume decreases, so particles must pass out of the right side of the control volume, again with no particle movement far from the blade at the left side of the control volume. Hence, there is a local horizontal displacement of particles at the blade, but particles remain stationary far from the blade. Of course, when the bump passes the periodic boundary, some particles also cross the periodic boundary with the bump. In fact, the volume of particles crossing the periodic boundary with the bump during each pass equals the volume of particles in the bump.

Before considering deep beds in the next section, we note that a streamwise segregation instability is observed at large N in cases where h and h/h_b are small, that is, cases where the bed is shallow and the blade is relatively tall. For example, long after the system has apparently stopped segregating vertically for $h = 5.7d_L$ and $h/h_b = 2.5$, a streamwise variation in the thickness of the segregated layers develops, as shown in Fig. 12. The amplitude of the local variation in layer thickness is a significant fraction of the bed height. Note also that the entire pattern is displaced in the direction of the blade motion on each pass. A similar and possibly related phenomenon is observed in the formation of washboard-like bump patterns when a wheel is repeatedly driven over a granular surface [31,32]. Here, the wavelength of the instability in Fig. 12 is approximately half the length of the bed. We leave a detailed investigation of this streamwise segregation phenomenon to a future study.

B. Deep beds

We now consider deep bed systems where the effect of the blade is localized near the blade such that the motion of the blade causes minimal disturbance to the bed surface. This is in contrast to shallow systems where the bed surface is substantially raised by the passage of the blade, i.e., a large bump is formed as shown in Fig. 12. For deep beds, the bed depth is large, both in absolute terms as well as relative to the blade height (e.g., for $h/d_L = 11$, 16.3, and $h/h_b = 10$).

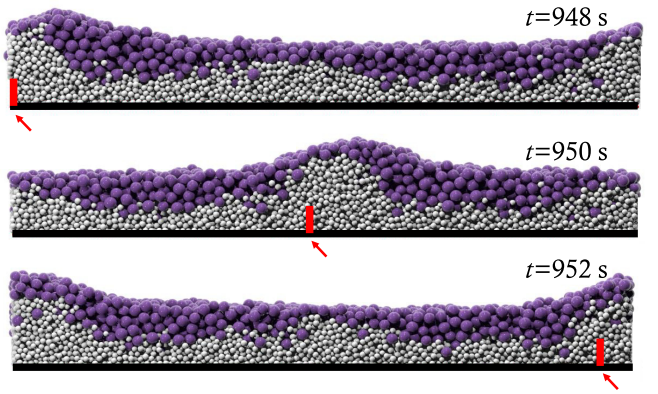

FIG. 12. Streamwise segregation instability with wavelength $L_z/2$ and manifested as variation in the segregated layer thickness for $h = 5.7d_L$ and $h/h_b = 2.5$ as the blade passes from left to right through the bed at $N = 150$. Red arrows indicate the blade position in each frame.

The segregation and kinematics described so far change qualitatively for deep bed systems. To illustrate this point, Fig. 13 plots the segregation metric Y_{CM} versus N for $h/h_b = 10$ for both a shallow bed ($h = 5.7d_L$, same data as in Fig. 6) and a deep bed ($h = 11d_L$) along with best fits to Eq. (2). It is clear from the figure that the data for $h = 11d_L$ is no longer well described by the exponential fit using Eq. (2). Beyond the poor fit to the data, the characteristic number of passes τ from the fit is 166 for the associated value of $\sqrt{gh^5}/(v_b h_b \bar{d}) = 1857$, which is nearly three times greater than the value predicted by the linear relationship shown in Fig. 8.

To explore why deep bed segregation differs from the shallow bed cases discussed in the previous section, we first examine Fig. 14, which shows side-view images of a deep

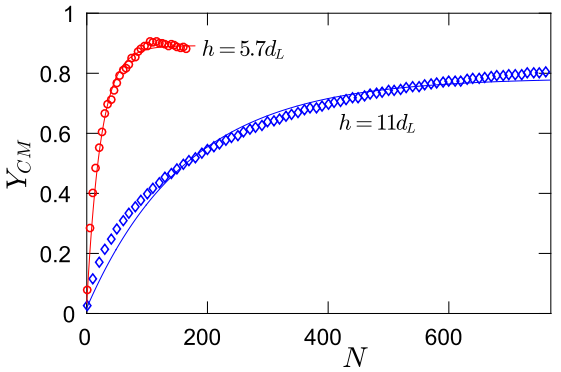

FIG. 13. Fits to Eq. (2) (solid curves) indicate that the exponential dependence of the segregation metric Y_{CM} on number of passes N for shallow beds (e.g., $h = 5.7d_L$ and $h/h_b = 10$, red) breaks down in a deep bed ($h = 11d_L$ and $h/h_b = 10$).

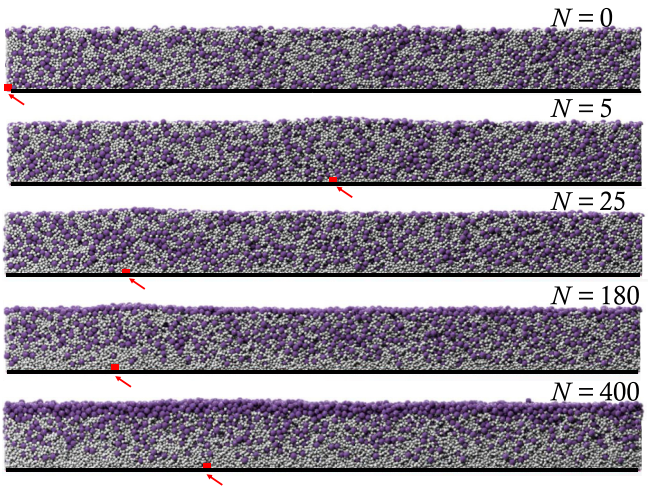

FIG. 14. Segregation evolution with number of passes N for a deep bed case with $h = 11d_L$, $h_b = 1.1d_L$, and $h/h_b = 10$. Red arrows indicate the blade position in each frame.

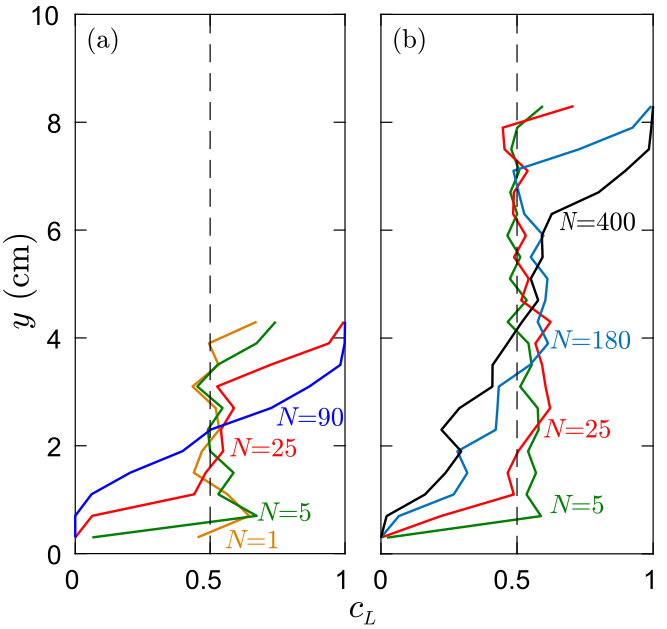

FIG. 15. Concentration of large particles, c_L, vs position above the bottom wall, y, at various numbers of passes N for (a) $h = 5.7d_L$, $h/h_b = 10$ and (b) $h = 11d_L$, $h/h_b = 10$.

bed as the number of passes increases. The most noticeable difference with the shallow bed case (see Fig. 3) is the much smaller bump above the blade in the deep bed case. Much slower segregation is also evident. At $N = 25$, the only obvious segregation is in a thin layer of small particles at the bottom wall. Otherwise, the particles are well mixed. At $N = 180$, a layer of large particles is evident on the surface. The segregation of large particles at the bed surface can be attributed to the passage of the very shallow bump due to the presence of the submerged blade, as discussed earlier. However, there remains a thick zone of mixed particles having a concentration similar to the initial concentration between the bottom layer of small particles and the top layer of large particles. By $N = 400$ significant segregation has occurred throughout the bed with a layer of nearly pure small particles at the bottom wall and a layer of nearly pure large particles at the free surface, though the layer of mixed particles persists in between.

We next compare concentration profiles through the bed depth for a shallow and a deep bed with increasing N. To calculate the concentration, the bed is divided into 4 mm high horizontal layers (bins) spanning the bed width and excluding the localized region affected by the blade. The concentration profiles of large particles c_L and small particles c_S are calculated once per pass for each horizontal bin. Figure 15 shows the depthwise concentration profiles of large particles for a shallow bed case ($h = 5.7d_L$) and the deep bed case ($h = 11d_L$), both with $h/h_b = 10$ as in Fig. 13. In the shallow bed [Fig. 15(a)], the initial ($N = 1$) concentration of large particles is approximately 0.5 throughout the depth of the bed. The concentration is slightly less than 0.5 nearest the bottom wall and slightly more than 0.5 just above it, reflecting the layer of small particles that forms on the bottom wall during filling as described earlier. At $N = 25$, $c_L = 0$ at the bottom of the bed as large particles have been depleted, while $c_L = 1$ at the free surface of the bed where large particles are segregating. By $N = 90$, the system is substantially segregated with small particles in a layer at the bottom ($c_L = 0$), large particles in a layer at the top ($c_L = 1$), and an extended gradient in concentration reflecting the diffuse interface between the two layers.

For the deep bed case in Fig. 15(b), the degree of segregation at $N = 5$ near the bottom wall and at the free surface is similar to the shallow bed case. At $N = 25$, $c_L = 0$ immediately above the bottom wall, but $c_L \approx 0.5$ for $0.012 < y < 0.075$ m, reaching $c_L \approx 0.7$ only near the free surface. The large well-mixed region persists for many passes. As N increases, this region starts further above the bottom wall and ends further from the free surface, where c_L approaches 1 as the large particle layer thickens. By $N \approx 400$, the $c_L \approx 0.5$ layer is replaced by a gradually varying concentration of large particles between layers of mostly small particles at the bottom wall and mostly large particles at the free surface.

Lastly, we compare the deep bed velocity field shown in Fig. 16 to the shallow bed cases in Fig. 9 for nearly the same absolute blade height ($h_b/d_L = 1.14$, $h/h_b = 5$, and $h = 5.7d_L$, middle panel) and the same relative blade height ($h_b/d_L = 0.57$, $h/h_b = 10$, and $h = 5.7d_L$, bottom panel). To aid the comparison, an expanded view at the same scale as in Fig. 9 is shown in the upper portion of Fig. 16 with the horizontal blue dashed line indicating the approximate bed depth h in the shallow bed case. For similar absolute blade height ($h_b/d_L \sim 1$), the vector magnitudes for the shallow bed are significantly larger in the blade vicinity than in the deep bed case, which could be due to the larger overburden pressure in the latter. However, for the same relative blade height ($h/h_b = 10$), the vector magnitudes in the blade vicinity are similar in both cases. Although the velocity field extends well above the blade in the deep bed case in Fig. 16, the recirculation zone is more localized near the blade than in the shallow bed case. As a result, the downward flow in the region behind the blade is not as strong. Hence, the segregation that

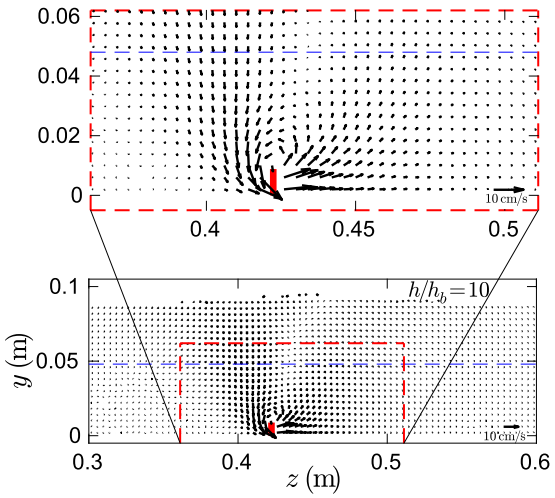

FIG. 16. Velocity vectors for $h = 11d_L$, $h/h_b = 10$, and $h_b/d_L = 1.1$ at $N = 5$. Velocity vectors are similar to those in Fig. 9 ($h/h_b = 5$, $h/h_b = 10$) for the shallow bed. The horizontal dashed blue line corresponds to the bed depth in Fig. 9 for these parameters.

occurs in the layer immediately above the recirculation zone in the deep bed case, which corresponds to the region that remains mixed in Fig. 15(b), is relatively much slower. In spite of this, the value for $\overline{|\mathbf{v}|}/v_b$ (averaged through the depth of the bed and a lateral distance of $3.1h$ centered on the blade) fits the relation shown in Fig. 10 (filled data points), indicating that v_{char} remains proportional to $v_b h_b/h$ in deep beds.

IV. CONCLUSIONS

In this paper, we have explored segregation induced by a submerged moving blade in a size-bidisperse particle bed. When a blade moves through an initially well-mixed bed of size-bidisperse particles, the particles segregate, after repeated passes, to form a layer of large particles above a layer of small particles, consistent with segregation patterns observed in bladed mixers [17,27].

The final segregation state is approached asymptotically and is well fit for shallow beds by an exponential model for a segregation metric having a characteristic number of passes, or "time constant," τ. The characteristic number of passes increases with both the absolute bed depth and the height of the bed relative to the blade height. While the final segregation state is also approached asymptotically for deep beds, the same exponential model does not characterize the evolution toward a segregated state as well, most likely because of a relatively thick layer of slowly segregating mixed particles between a layer of small particles near the bottom wall and a layer of large particles at the free surface.

As the blade moves through the bed of particles, it creates a finite zone of disturbance in front of and behind the blade beyond which particles remains stationary. Segregation likely occurs by a sieving mechanism where small particles fall in voids created when the particles are disturbed locally by the movement of the blade. In shallow beds, the localized region of moving particles around the blade extends to the free surface, where a bump is formed above and slightly in front of the blade. The volume of the bump corresponds to the volume of particles that are displaced in the streamwise direction with each pass of the blade. As the blade moves, particles flow down the back side of the bump resulting in additional segregation at the free surface.

A different situation arises for systems with large bed depth to blade height ratios h/h_b, as well as large bed depth h, i.e., systems with large bed depth relative to both the particle diameter and the blade height. While these "deep" systems segregate, the time to achieve steady state segregation is much longer than for the shallow cases. This occurs because, while velocity disturbances extend through the depth of the bed above the blade, they are relatively weak at large distances from the blade. Furthermore, the bump above the blade is quite small for deep beds, thereby minimizing the surface segregation that occurs as particles flow down the back side of the bump. Hence, the large particles that segregate upward from the bottom where large velocities occur near the blade can only gradually move upward through the remainder of the bed above the blade. Similarly, small particles move slowly downward above the blade due to the relatively small velocity disturbances there. Hence, relatively rapid segregation occurs in the first few passes for both shallow and deep beds because of the large relative velocity in the immediate vicinity of the blade and the bump at the free surface, but segregation slows in deep beds as particles migrate through the thick layer of mixed particles between the top of the blade and the free surface.

There are several questions remaining. First, we have only begun to explore the segregation parameter space. The segregation likely also depends on various other parameters including the relative particle concentrations, the particle size ratio, the absolute particle sizes d_L and d_S, and the blade velocity, particularly at higher velocities. The effect of particle shape and frictional properties should also be studied. The blade inclination can also be modified to study how it impacts segregation as in bladed mixer studies [15,17,19,26,27].

Perhaps of more importance is to relate the segregation due to the blade to the various models for segregation. Clearly, the segregation mechanism is related to the disruption of the static bed of particles by the blade. Near the surface of the bed, the bump results in particle segregation much like that which occurs as particles flow down a sloped free surface, which has been explained in terms of the free surface angle [10] and the local shear rate [8,9]. However, deep in the bed the segregation mechanism is less clear. Mechanisms based on both the local shear rate [6,8] and the local stress field [11] have been proposed, but it is not clear how these mechanisms relate to segregation due to a subsurface blade or even to each other. Unlike the canonical chute, heap, and tumbler flows frequently used to study segregation, segregation from a moving subsurface blade may allow a better understanding of how these various mechanisms may interact.

ACKNOWLEDGMENTS

The authors thank A. M. Fry for several useful discussions, as well as A. Lin and D. Lee for their contribution to the annular experimental apparatus.

APPENDIX: DEM METHODS

Particle interactions are modeled using a linear spring dashpot normal force and a combination of linear spring and Coulomb friction tangential force using code previously developed in our laboratory and validated against experiments and other DEM codes [9,29,33]. The bottom wall and blade are made up of particles having the same properties as bed particles but with a smaller diameter, $d_{\text{wall}} = 2.2$ mm, to provide a rough surface. Interactions between these surfaces and bed particles are modeled using the same contact equations. For particles in contact, the normal force is

$$\boldsymbol{f}_{ij}^{n} = [k_n\zeta - 2\gamma_n m_{\text{eff}}(\mathbf{V}_{ij}\cdot\hat{\mathbf{r}}_{ij})]\hat{\mathbf{r}}_{ij}$$

and the tangential force is

$$\boldsymbol{f}_{ij}^{t} = \min\left\{|k_t\beta - 2\gamma_t m_{\text{eff}}(\mathbf{V}_{ij}\times\hat{\mathbf{r}}_{ij})|,\ \left|\mu\mathbf{F}_{ij}^{n}\right|\right\}\text{sgn}(\beta)\hat{\mathbf{s}},$$

as in previous work [34–36]. Here k_n and k_t represent the normal and tangential spring stiffnesses, ζ and β are the normal and tangential relative displacements, and γ_n and γ_t are the normal and tangential damping coefficients, respectively. The unit vector in the tangential direction is $\hat{s}$. $\mathbf{V}_{ij} = \mathbf{V}_i - \mathbf{V}_j$ denotes the relative velocity of two contacting particles i and j, and $\hat{\mathbf{r}}_{ij}$ is the unit vector between particle centers. The effective mass is $m_{\text{eff}} = m_i m_j/(m_i + m_j)$. To model static tangential contact [37], the static friction force is calculated using the tangential displacement $\beta(t) = \int_{t_o}^{t} V_{ij}^{t} dt$, where V_{ij}^{t} is the instantaneous tangential velocity between contacting particle surfaces, t is the time, and t_o is the time of initial contact [35]. In the case of sliding tangential contact, the friction coefficient $\mu = 0.4$ for both particle-particle and particle-wall/blade interactions. The specified collision parameters are related to the contact time, t_c, and the restitution coefficient, ε, by $k_n = [(\pi/t_c)^2 + \gamma_n^2]m_{\text{eff}}$ and $\gamma_n = -\ln(\varepsilon)/t_c$. Tangential parameters are $k_t = 2/7k_n$ and $\gamma_t = 2/7\gamma_n$ [35]. In this work, $\varepsilon = 0.8$ and $t_c = 0.5 \times 10^{-3}$ s. This value of t_c lies within the range sufficient for modeling hard spheres, consistent with previous simulations [29]. The symplectic Euler integration algorithm is used to update particle positions and velocities [38].

[1] A. D. Rosato, D. L. Blackmore, N. Zhang, and Y. Lan, Chem. Eng. Sci. **57**, 265 (2002).
[2] A. Kudrolli, Rep. Prog. Phys. **67**, 209 (2004).
[3] J. M. Ottino and D. V. Khakhar, Annu. Rev. Fluid Mech. **32**, 55 (2000).
[4] J. M. N. T. Gray, Annu. Rev. Fluid Mech. **50**, 407 (2018).
[5] P. B. Umbanhowar, R. M. Lueptow, and J. M. Ottino, Annu. Rev. Chem. Biomol. Eng. **10**, 129 (2019).
[6] S. B. Savage and C. K. K. Lun, J. Fluid Mech. **189**, 311 (1988).
[7] L. Jing, C. Y. Kwok, and Y. F. Leung, Phys. Rev. Lett. **118**, 118001 (2017).
[8] Y. Fan, C. P. Schlick, P. B. Umbanhowar, J. M. Ottino, and R. M. Lueptow, J. Fluid Mech. **741**, 252 (2014).
[9] C. P. Schlick, Y. Fan, A. B. Isner, P. B. Umbanhowar, J. M. Ottino, and R. M. Lueptow, AIChE J. **61**, 1524 (2015).
[10] J. Gray and A. R. Thornton, Proc. R. Soc. Ai **461**, 1447 (2005).
[11] K. M. Hill and D. S. Tan, J. Fluid Mech. **756**, 54 (2014).
[12] J. A. Drahun and J. Bridgwater, Powder Technol. **36**, 39 (1983).
[13] M. Shearer, J. M. N. T. Gray, and A. R. Thornton, Eur. J. Appl. Math. **19**, 61 (2008).
[14] Y. Fan, K. V. Jacob, B. Freireich, and R. M. Lueptow, Powder Technol. **312**, 67 (2017).
[15] B. Remy, J. G. Khinast, and B. J. Glasser, AIChE J. **55**, 2035 (2009).
[16] B. Remy, B. J. Glasser, and J. G. Khinast, AIChE J. **56**, 336 (2010).
[17] Y. C. Zhou, A. B. Yu, and J. Bridgwater, J. Chem. Technol. Biotechnol. **78**, 187 (2003).
[18] J. K. Kouwenhoven and R. Terpstra, J. Agric. Eng. Res. **15**, 129 (1970).
[19] B. Remy, T. M. Canty, J. G. Khinast, and B. J. Glasser, Chem. Eng. Sci. **65**, 4557 (2010).
[20] S. Radl, D. Brandl, H. Heimburg, B. J. Glasser, and J. G. Khinast, Powder Technol. **226**, 199 (2012).
[21] R. D. Maladen, Y. Ding, P. B. Umbanhowar, A. Kamor, and D. I. Goldman, J. R. Soc., Interface **8**, 1332 (2011).
[22] N. Gravish, P. B. Umbanhowar, and D. I. Goldman, Phys. Rev. Lett. **105**, 128301 (2010).
[23] M. S. Siraj, S. Radl, B. J. Glasser, and J. G. Khinast, Powder Technol. **211**, 100 (2011).
[24] D. Bagster and J. Bridgwater, Powder Technol. **3**, 323 (1969).
[25] R. L. Stewart, J. Bridgwater, and D. J. Parker, Chem. Eng. Sci. **56**, 4257 (2001).
[26] S. L. Conway, A. Lekhal, J. G. Khinast, and B. J. Glasser, Chem. Eng. Sci. **60**, 7091 (2005).
[27] B. Remy, J. G. Khinast, and B. J. Glasser, Chem. Eng. Sci. **66**, 1811 (2011).
[28] N. Khola and C. Wassgren, Powder Technol. **288**, 441 (2016).
[29] A. M. Fry, P. B. Umbanhowar, J. M. Ottino, and R. M. Lueptow, Phys. Rev. E **97**, 062906 (2018).
[30] F. da Cruz, S. Emam, M. Prochnow, J.-N. Roux, and F. Chevoir, Phys. Rev. E **72**, 021309 (2005).
[31] N. Taberlet, S. W. Morris, and J. N. McElwaine, Phys. Rev. Lett. **99**, 068003 (2007).
[32] A. F. Bitbol, N. Taberlet, S. W. Morris, and J. N. McElwaine, Phys. Rev. E **79**, 061308 (2009).
[33] H. Xiao, J. M. Ottino, R. M. Lueptow, and P. B. Umbanhowar, Phys. Rev. E **96**, 040902(R) (2017).
[34] P. A. Cundall and O. D. L. Strack, Geotechnique **29**, 47 (1979).
[35] J. Shäfer, S. Dippel, and D. E. Wolf, J. Phys. I **6**, 5 (1996).
[36] G. H. Ristow, *Pattern Formation in Granular Materials*, Springer Tracts in Modern Physics (Springer-Verlag, Berlin, 2000), Vol. 164.
[37] D. C. Rapaport, Phys. Rev. E **65**, 061306 (2002).
[38] A. Cromer, Am. J. Phys. **49**, 455 (1981).